Dalton Transactions

ROYAL SOCIETY OF CHEMISTRY

PAPER

View Article Online
View Journal | View Issue

Open Access Article. Published on 02 February 2023. Downloaded on 10/19/2023 4:08:06 PM.
This article is licensed under a Creative Commons Attribution 3.0 Unported Licence.

Check for updates

Cite this: *Dalton Trans.*, 2023, **52**, 3203

Elucidating the exchange interactions in a {$Gd^{III}Cu_4^{II}$} propellor†

María José Heras Ojea, ‡[a] Claire Wilson, [a] Jordi Cirera, [b] Hiroki Oshio, [c] Eliseo Ruiz[b] and Mark Murrie *[a]

Received 2nd December 2022,
Accepted 1st February 2023

DOI: 10.1039/d2dt03901j

rsc.li/dalton

The multinucleating ligand 2,2′-(propane-1,3-diyldiimino)bis[2-(hydroxymethyl)-propane-1,3-diol] (bis–tris propane, H_6L) is used in the design of a new family of 3d–4f complexes that display an unusual {$LnCu_4$} four-blade propeller topology. We report the synthesis, structure and magnetic characterisation of $[LnCu_4(H_4L)_4](Cl)_2(ClO_4)\cdot 6CH_3OH$, where Ln = Gd (**1**), Tb (**2**), Dy (**3**), La (**4**). Previously we have used CH_3COO^- and NO_3^- as co-ligands with bis–tris propane, but here the use of Cl^- and ClO_4^- leads to coordination of four {$Cu(H_4L)$} units around the central Ln ion. A magneto-structural analysis reveals that the geometrical arrangement of the Cu(II) centres defined by the H_4L^{2-} ligands controls the magnetic communication between the different metal centres. DFT calculations performed on the isotropic (Gd) and diamagnetic (La) systems **1** and **4** help to unravel the intriguing exchange interactions.

Introduction

The assembly of heterometallic coordination complexes is a fascinating synthetic challenge that remains a hot topic in inorganic chemistry.[1] The majority of this work has been driven by interest in the magnetic properties of 3d–4f complexes, including the study of single-molecule magnets.[2,3] Regarding the understanding of 3d–4f magnetic exchange interactions, Gd/Cu-based heterometallic complexes have been the most widely investigated, since the analysis of their magnetic properties is simplified compared to other lanthanide ions due to the spin-only contribution of Gd(III) ions (L = 0).[3a,c,4]

We have a long-standing interest in the use of polydentate ligands to direct the assembly of heterometallic complexes.[1d,5,6] The bis–tris propane ligand {H_6L = 2,2′-(propane-1,3-diyldiimino)bis[2-(hydroxymethyl)propane-1,3-diol]} has a particular affinity for binding 3d ions in the synthesis of 3d–4f complexes and this can provide a flexible structure-directing effect (see Scheme 1).[5,6] In previous work on {$Ln_2Cu_3(H_3L)_2X_n$} (X = OAc^-, NO_3^-) complexes we investigated the effect of using acetate or nitrate co-ligands.[6] Subsequently, we have explored alternative auxiliary ligands (ClO_4^-, Cl^-) and we now show that this allows the synthesis of a completely new family of Cu/4f bis–tris propane complexes $[LnCu_4(H_4L)_4](Cl)_2(ClO_4)\cdot 6CH_3OH$ (Ln = Gd, Tb, Dy, La) with an unusual four-blade propeller topology. A magneto-structural analysis reveals that the Cu(II) coordination motif defined by the H_4L^{2-} ligands controls the magnetic communication between the different metal centres. DFT calculations performed on the

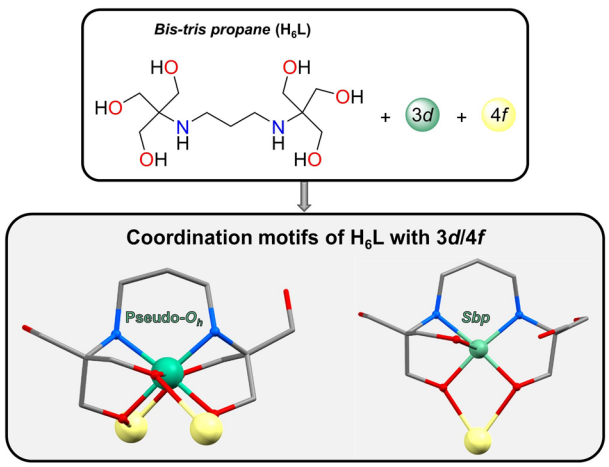

Scheme 1 Bis–tris propane (H_6L) and some of the possible coordination motifs (Sbp = square-based pyramidal) in 3d–4f heterometallic complexes.

[a]*School of Chemistry, University of Glasgow, University Avenue, Glasgow G12 8QQ, UK. E-mail: mark.murrie@glasgow.ac.uk*
[b]*Departament de Química Inorgànica i Orgànica and Institut de Recerca de Química Teòrica i Computacional, Universitat de Barcelona, Diagonal 645, 08028 Barcelona, Spain*
[c]*State Key Laboratory of Fine Chemicals, Dalian University of Technology, 2 Linggong Rd., 116024 Dalian, China*

†Electronic supplementary information (ESI) available: Crystallographic details, EDX, magnetic and DFT studies. CCDC **1**: 1988774; **2**: 1988775; **3**: 1988776 and **4**: 1988777. For ESI and crystallographic data in CIF or other electronic format see DOI: https://doi.org/10.1039/d2dt03901j

‡Current address: Department of Pure and Applied Chemistry, University of Strathclyde, Glasgow G1 1XL, U.K.

Open Access Article. Published on 02 February 2023. Downloaded on 10/19/2023 4:08:06 PM.
This article is licensed under a Creative Commons Attribution 3.0 Unported Licence.

isotropic (Gd) and diamagnetic (La) systems **1** and **4** are used to support the experimental magnetic properties and help to unravel the intriguing Cu···Gd exchange interactions in **1**.

Experimental section

Materials and physical methods

All reagents and solvents were obtained from commercial suppliers and used without further purification. Perchlorate salts are potentially explosive, and so the compounds should be prepared in small quantities and handled with care.

Crystallographic data for **1–3** were collected at 100 K using Mo-Kα radiation (λ = 0.71073 Å). For **4**, Cu-Kα radiation was used (λ = 1.54184 Å). For **1** a Bruker APEXII CCD diffractometer with an Oxford Cryosystems device mounted on a sealed tube generator was used. For **2** a Bruker–Nonius Kappa CCD diffractometer with an Oxford Cryosystems device mounted on a sealed tube generator was used. For **3** a Bruker D8 VENTURE diffractometer equipped with a Photon II CMOS detector with an Oxford Cryosystems *n*-helix device mounted on a IμS 3.0 (dual Cu and Mo) microfocus sealed tube generator was used. For **4** a Rigaku Oxford Diffraction SuperNova equipped with an AtlasS2 CCD detector and an Oxford Cryosystems device was used. All the structures were solved using SUPERFLIP[7] and refined using full-matrix least squares refinement on F^2 using SHELX2014[8] within OLEX2.[9] Hydrogen atoms were placed in geometrically calculated positions and refined as part of a riding model, except those from molecules of methanol and from the uncoordinated OH groups of the H_4L^{2-} ligands, which were refined as part of a rigid rotating group. The perchlorate anion is half occupied and overlaps with a half occupied MeOH molecule, with one of the oxygen atoms forming part of both the perchlorate (O4) and the MeOH oxygen (O5). These were constrained to have the same position and *adps*. One other MeOH is also half occupied. In addition, the O1S atom of one of the methanol molecules in **4** was modelled over two partially occupied sites with competitively refined occupancies of 0.9(9) : 0.1(1). Compounds **1–4** desolvate and show a slight hygroscopic tendency, similar to that observed in previously published complexes obtained using H_6L as a ligand, which precludes the use of powder X-ray diffraction.[6,10]

Energy Dispersive X-ray (EDX) experiments for **1** were carried out using a Philips XL 30 Environmental Scanning Electron Microscope (ESEM) at different magnifications. To remove complications due to charging, samples were gold-coated using a vacuum electric sputter coater (POLARON SC 7640) prior to analysis. The images were taken using a W-Kα (57 981.77 eV) radiation with a Secondary Electron detector and Oxford Instruments INCA 250Xact10 EDX detector. EDX analysis was performed on a on a bulk crystalline sample of **1** (Fig. S1†). The average Gd : Cu ratio found is 1 : 4, which is consistent with that established by single-crystal XRD thus ruling out any Cu-monomeric impurity. Further EDX map analysis for Cu and Gd was performed to establish the distribution of the metal ions in the sample (Fig. S1† top, left). This reveals the even distribution of Gd/Cu in the crystalline bulk sample (Avg. Atomic% Gd : Cu is 1.01 : 4.06). The IR spectra were measured using a FTIR-8400S SHIMADZU IR spectrophotometer. The microanalyses were performed by the analytical services of the School of Chemistry at the University of Glasgow. Magnetic measurements were performed on polycrystalline samples, that were powdered and restrained in eicosane, using a Quantum Design MPMS-XL or MPMS-5S SQUID magnetometer. Data were corrected for the diamagnetic contribution of the sample holder and eicosane by measurements and for the diamagnetism of the compounds. Ac susceptibility data were collected on cooling with an ac drive field of 3 Oe oscillating at frequencies between 1 and 1500 Hz.

Computational details

To calculate the exchange interactions,[11] a phenomenological Heisenberg Hamiltonian was used, excluding the terms related to magnetic anisotropy (D and E zero-field splitting parameters) to describe the exchange coupling in the polynuclear complex:

$\mathcal{H} = -\sum_{a<b} J_{ab}\hat{S}_a\hat{S}_b$ where $\hat{S}_a$ and $\hat{S}_b$ are the spin operators of the different magnetic centres. The J_{ab} parameters are the pairwise coupling constants between the paramagnetic centers of the molecule. In order to solve the system, we need to calculate the energy of n + 1 spin distributions for a given system with n different exchange coupling constants. In our particular case, seven calculations were done for system **1** and four calculations for system **4**. For system **1** ($[GdCu_4(H_4L)_4]^{3-}$), they correspond to the high-spin S_z = 11/2 solution, four S = 7/2 solutions corresponding to the spin inversion of two copper centres, and two S = 9/2 solutions corresponding to the spin-inversion of one copper centre. For system **4** ($[LaCu_4(H_4L)_4]^{3-}$), they correspond to the high-spin S_z = 2 solution, one S = 1 solution corresponding to the inversion of one copper centre and two S = 0 solutions corresponding to the inversion of two copper centres (see Table S7†). These energy values allowed us to build a system of n equations in which the $\mathcal{J}$ values are the unknowns. All calculations were performed using Gaussian09 (rev D01)[12] with the hybrid functional B3LYP,[13] using a guess function generated with the help of the fragments option, which employs a procedure that allows us to individually assign local electronic structures to atoms and/or ligands. A triple-ζ all electron Gaussian basis set was used for all the atoms, including polarization functions for the Cu centres.[14] An all electron basis set was also used for the Gd and La atoms. In order to include 2nd order scalar relativistic effects in the calculations, a Douglas–Kroll–Hess Hamiltonian (DKH) was used.[15]

Synthetic methods

$[GdCu_4(H_4L)_4](Cl)_2(ClO_4)\cdot 6CH_3OH$ (1). H_6L (1.41 g, 5 mmol) and Et_3N (1.39 mL, 10 mmol) were consecutively added to a solution of $GdCl_3\cdot 6H_2O$ (0.38 g, 1 mmol) in MeOH (154 mL), resulting in a white suspension. $Cu(ClO_4)_2\cdot 6H_2O$ (1.86 g, 5 mmol) was then added, and immediately dissolved, giving a

 This journal is © The Royal Society of Chemistry 2023

Open Access Article. Published on 02 February 2023. Downloaded on 10/19/2023 4:08:06 PM.
This article is licensed under a Creative Commons Attribution 3.0 Unported Licence.

dark violet solution. The solution was stirred and heated to 60 °C for 3 h. The initial dark violet solution turned purple. Purple plate-like single crystals suitable for X-ray diffraction were obtained by slow diffusion of Et_2O into the reaction solution over one week. Yield 74% (1.26 g). IR: ν (cm^{-1}) = 3227, 2880, 1738, 1425, 1267, 1040, 1074, 878, 623. Elemental analysis ($[GdCu_4(H_4L)_4](Cl)_2(ClO_4)\cdot 3.5H_2O$) [%], found: C 29.79, H 5.72, N 6.24; calc: C 29.92, H 5.88, N 6.34.

$[TbCu_4(H_4L)_4](Cl)_2(ClO_4)\cdot 6CH_3OH$ (2). The same synthetic procedure described for **1** was followed, but using $TbCl_3\cdot 6H_2O$ (0.46 g, 1.2 mmol) instead of $GdCl_3\cdot 6H_2O$. Yield 71% (1.49 g). IR: ν (cm^{-1}) = 3219, 2882, 1738, 1425, 1072, 1013, 880, 673, 623. Elemental analysis ($[TbCu_4(H_4L)_4](Cl)_2(ClO_4)\cdot 5.5H_2O$) [%], found: C 28.9, H 5.55, N 6.03; calc: C 29.3, H 5.98, N 6.21.

$[DyCu_4(H_4L)_4](Cl)_2(ClO_4)\cdot 6CH_3OH$ (3). The same synthetic procedure described for **1** was followed, but using $DyCl_3\cdot 6H_2O$ (0.48 g, 1.2 mmol) instead of $GdCl_3\cdot 6H_2O$. Yield 42% (0.91 g). IR: ν (cm^{-1}) = 3212, 2880, 1613, 1425, 1267, 1076, 1042, 876, 673. Elemental analysis ($[DyCu_4(H_4L)_4](Cl)_2(ClO_4)\cdot 3H_2O$) [%], found: C 29.7, H 5.85, N 6.17; calc: C 29.64, H 5.93, N 6.25.

$[LaCu_4(H_4L)_4](Cl)_2(ClO_4)\cdot 6CH_3OH$ (4). The same synthetic procedure described for **1** was followed, but using $LaCl_3\cdot H_2O$ (0.05 g, 0.1 mmol) instead of $GdCl_3\cdot 6H_2O$. Yield 86% (0.20 g). IR: ν (cm^{-1}) = 3231, 2880, 1643, 1464, 1072, 1013, 880, 673, 623. Elemental analysis ($[LaCu_4(H_4L)_4](Cl)_2(ClO_4)\cdot 5.75H_2O$) [%], found: C 29.70, H 6.02, N 6.11; calc: C 29.55, H 6.06, N 6.27.

Results and discussion

Applying a similar synthetic route to that we used previously for the $\{Ln_2Cu_3(H_3L)_2X_n\}$ series of complexes we were able to synthesise a new family of Cu/4f complexes. The $[LnCu_4(H_4L)_4](Cl)_2(ClO_4)\cdot 6CH_3OH$ systems (Ln being Gd (**1**), Tb (**2**), Dy (**3**) or La (**4**)) display an unusual and completely different topology to that observed when OAc^- and NO_3^- co-ligands were used. The oxophilic nature of the lanthanides may explain to some extent the new metal arrangement, as the substitution of the oxygen-donor co-ligands (X = OAc^-, NO_3^-) used for $\{Ln_2Cu_3(H_3L)_2X_n\}$ complexes by typically non-coordinating ClO_4^- and typically monodentate Cl^- co-ligands could promote the coordination of the $\{Cu(H_4L)\}$ units around the Ln ion in **1–4**.

X-ray crystallographic analysis

Selected crystallographic details for **1–4** are shown in Table 1. The complexes crystallise in the monoclinic space group *C*2/*c*. The asymmetric unit of **1–4** contains one half-molecule of $[LnCu_4(H_4L)_4]^{3+}$, a chloride anion, a half-perchlorate anion, and three lattice molecules of methanol. As the cations $[LnCu_4(H_4L)_4]^{3+}$ of **1–4** are isostructural, the following description applies to all the complexes.

The structure of $[LnCu_4(H_4L)_4]^{3+}$ contains four $\{Cu(H_4L)\}$ units surrounding one central Ln(III) ion. Each $\{Cu(H_4L)\}$ moiety binds to the Ln centre by the coordination of two μ-O from the doubly deprotonated H_4L^{2-} ligand (see Fig. 1). The symmetry analyses of the octa-coordinated Ln(III) ions were performed by calculating Continuous Shape Measures

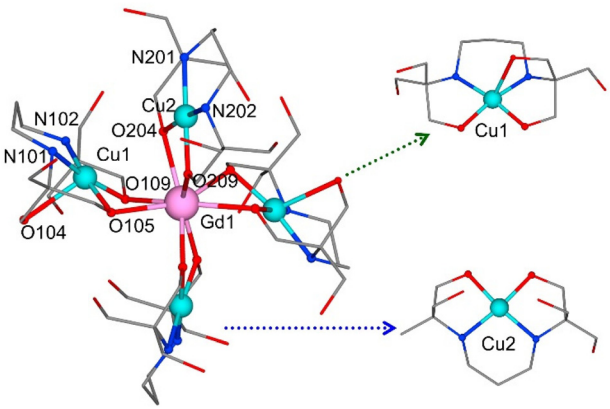

Fig. 1 Structure of the cation (left) and detail (right) of **1**. C, grey; Cu, turquoise; Gd, pink; N, blue; O, red. Hydrogen atoms, solvent and counterion molecules are omitted for clarity. Only crystallographically unique Cu, Gd, N and O atoms are labelled.

Table 1 Crystal data and structure refinement parameters of complexes **1–4**

Complex	**1** (Gd)	**2** (Tb)	**3** (Dy)	**4** (La)
T/K	100(2)	100(2)	100(2)	100(2)
Crystal system	Monoclinic	Monoclinic	Monoclinic	Monoclinic
Space group	*C*2/*c*	*C*2/*c*	*C*2/*c*	*C*2/*c*
a/Å, *b*/Å, *c*/Å	32.405(2), 11.0450(6), 25.0948(17)	32.4050(7), 11.0378(2), 25.0517(5)	32.254(4), 11.0373(2), 25.039(3)	32.5448(19), 11.0401(3), 25.2051(15)
β/°	125.610(3)	125.632(1)	125.646(4)	125.674(9)
V/Å^3	7302.0(8)	7282.9(3)	7243.6(15)	7356.7(9)
Z	4	4	4	4
ρ_{calc}/mg m^{-3}	1.724	1.7226	1.714	1.695
μ/mm^{-1}	2.150	2.216	2.283	7.460
F(000)	3916.0	3889.8	3800.0	3888.0
Reflections collected	48 082	12 292	40 413	11 988
Data/restraints/parameters	6489/484/499	6503/48/486	8961/462/498	6449/38/485
GOF on F^2	1.083	1.053	0.957	1.054
Final *R* indexes [$I \geq 2\sigma(I)$]	R_1 = 0.0492, wR_2 = 0.1003	R_1 = 0.0323, wR_2 = 0.0789	R_1 = 0.0402, wR_2 = 0.1128	R_1 = 0.0393, wR_2 = 0.1055
Final *R* indexes [all data]	R_1 = 0.0871, wR_2 = 0.1149	R_1 = 0.0458, wR_2 = 0.0842	R_1 = 0.0468, wR_2 = 0.1188	R_1 = 0.0410, wR_2 = 0.1073
Largest diff. peak/hole/e Å^{-3}	1.44/−0.98	1.06/−0.72	1.29/−0.85	1.29/−1.14

Open Access Article. Published on 02 February 2023. Downloaded on 10/19/2023 4:08:06 PM.
This article is licensed under a Creative Commons Attribution 3.0 Unported Licence.

(CShMs), giving square antiprism (D_{4d}) as the closest ideal geometry in the four complexes (see Table S1 of the ESI†).[16] Each Cu(II) ion occupies the inner $\{N_2O_2\}$ pocket of one H_4L^{2-} ligand, presenting two different coordination environments depending on the number of bonding O atoms (see Fig. 1). Therefore two Cu(II) ions display a square-planar (Sp) geometry due to the coordination of two N and two μ-O from H_4L^{2-}, whereas the two others show a distorted square-based pyramidal (Sbp) geometry (τ_{Cu} = 0.19 (**1**), 0.21 (**2**), 0.21 (**3**), 0.17 (**4**))[6,17] due to the coordination of an additional O–H_4L^{2-} atom. The intramolecular distances between the different metal centres vary from $d^{Avg}_{(Cu1\cdots Cu2)}$ = 4.761(5)–4.874(6) Å; $d^{Avg}_{(Cu\cdots Cu')}$ = 6.309(6)–6.471(6) Å; $d_{(Cu1\cdots Ln1)}$ = 3.242(8)–3.313(9) Å; and $d_{(Cu2\cdots Ln1)}$ = 3.295(4)–3.383(9) Å (see Table S2†). Two Cu–O–Ln average bridging angles can be distinguished considering the geometry of the Cu(II) ion. Consequently the Cu1–O–Ln angles lie between 93.95(6)° and 94.75(7)°, while the values for Cu2–O–Ln are notably larger (100.75(6)°–101.45(10)°). The complexes show the same trend for the Cu–O···O–Ln average torsion angles (see Table S3†): Cu1–O···O–Ln values are smaller (from 134.87(3)° to 136.68(1)°) compared to those displayed for Cu2–O···O–Ln (from 160.08(3)° to 161.06(1)°). The dependence of bridging angles and torsion angles related to the environment around the Cu centres is reasonable, as Cu2 is sterically more hindered than Cu1.

There is only one structure with a similar topology based on a $\{LnO_8Cu_4\}$ core, where the four Cu(II) ions enclose a central lanthanide.[18] However, the anionic complex $[Cu_4Ln(nd)_8]^{5-}$ (H_2nd = naphthalene-2,3-diol) has all the Cu(II) centres in a square-planar environment, whereas **1–4** show alternating square-planar and square-based pyramidal geometries. Given that relatively minor structural modifications can promote drastic changes in the overall magnetic properties of a complex, we have performed a magnetic study of the $[LnCu_4(H_4L)_4](Cl)_2(ClO_4)\cdot 6CH_3OH$ family along with DFT calculations of the Gd (**1**) and La (**4**) analogues.

Magnetic properties

The magnetic susceptibility of **1–4** were measured in an applied dc field of 1000 Oe from 290–1.8 K (see Fig. 2). The experimental values of $\chi_M T$ at room temperature for **1–4** are in agreement with those expected for four isolated Cu(II) ions (S_{Cu} = 1/2, g_{Cu} = 2.11) and one Ln(III) ion (Gd^{3+} for **1**; Tb^{3+} for **2**; Dy^{3+} for **3**; La^{3+} for **4**); see Table S4† for additional information. The g_{Cu} = 2.11 value used to calculate the expected $\chi_M T$ products is consistent with that determined by EPR studies in previous reported complexes presenting similar Cu(II) environments.[6,19] Compound **1** (Gd) displays some ferromagnetic coupling, as the experimental $\chi_M T$ product increases with decreasing temperature, reaching a maximum of 10.6 cm^3 mol^{-1} K at 20 K. Below 20 K the $\chi_M T$ value drops to 8.47 cm^3 mol^{-1} K at 1.8 K (*vide infra*).

In contrast, **2** (Tb) and **3** (Dy) display a moderate decrease in $\chi_M T$ between 290–15 K (from 13.5 cm^3 mol^{-1} K to 12.5 cm^3 mol^{-1} K for **2**, and 15.9 cm^3 mol^{-1} K to 15.0 cm^3 mol^{-1} K for **3**). This could be related to the depopulation of the Stark sub-

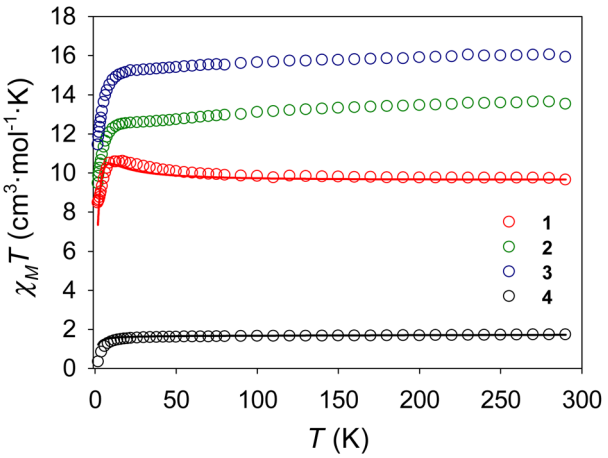

Fig. 2 Temperature dependence of $\chi_M T$ for **1** (Gd), **2** (Tb), **3** (Dy) and **4** (La) in an applied dc field of 1000 Oe. The solid lines correspond to the fit for **1** and **4** (see Electronic structure calculation section for details).

levels due to crystal field effects as the temperature is lowered. A sharp decrease then takes place, until the $\chi_M T$ products reach minima of 9.46 cm^3 mol^{-1} K (**2**) and 11.4 cm^3 mol^{-1} K (**3**) at 1.8 K. **4** (La) was studied in order to investigate possible weak interactions between the different Cu(II) ions, since La(III) is diamagnetic. $\chi_M T$ for **4** drops at low temperatures (below 20 K), reaching a minimum of 0.35 cm^3 mol^{-1} K at 2 K. This decrease is consistent with weak antiferromagnetic intramolecular Cu···Cu exchange in **4**, although we note that the presence of weak antiferromagnetic intermolecular interactions cannot be entirely discounted.

Several experimental and theoretical studies based on Cu/Ln complexes show the tendency of Cu···Gd centres to couple ferromagnetically.[3a–d] Previous work based on $\{Gd('O')_2Cu\}$ complexes reveals the relationship between the nature of the Cu···Gd interaction ($\mathcal{J}$) and the dihedral angle, here described as α.[3a] The dihedral angle (α) is defined by the planes formed by the atoms involved in the magnetic exchange (see Fig. 3). These studies show that the $\mathcal{J}$ value decreases when α becomes larger and may even display small negative values, *i.e.* weak antiferromagnetic exchange, when $\alpha \geq 40°$.[3a]

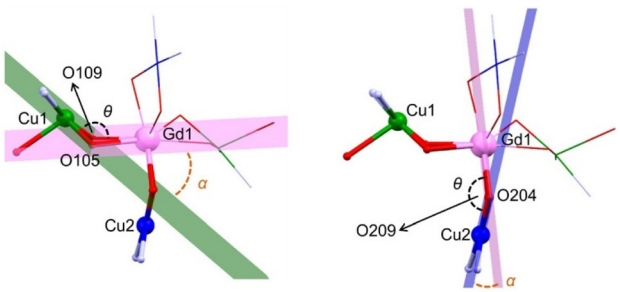

Fig. 3 Detail of the crystal structure of **1**. C, grey; Cu1, green; Cu2, blue; Gd, pale pink; N, lavender; O, red. The different planes are shown in green (O105–Cu1–O109), blue (O204–Cu2–O209), and pink (O105–Gd1–O109, O204–Gd1–O209). The dihedral (α) and the torsion angles (θ) are highlighted in orange and black, respectively.

This journal is © The Royal Society of Chemistry 2023

Open Access Article. Published on 02 February 2023. Downloaded on 10/19/2023 4:08:06 PM.
This article is licensed under a Creative Commons Attribution 3.0 Unported Licence.

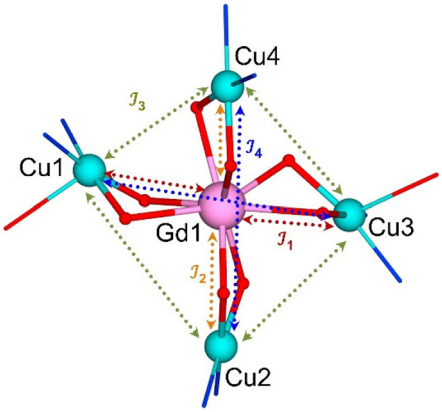

Fig. 4 Magnetic model used for the DFT calculations of **1** (Gd). The different exchange pathways are defined as $\mathcal{J}_1$ (Gd1–Cu1 and Gd1–Cu3), $\mathcal{J}_2$ (Gd1–Cu2 and Gd1–Cu4), $\mathcal{J}_3$ (*cis*-Cu) and $\mathcal{J}_4$ (*trans*-Cu). Further details are provided in the Experimental section.

For **1–4**, two non-equivalent Cu(II) atoms displaying different coordination environments can be distinguished, and thus two different Cu···Gd magnetic pathways could be expected (see Fig. 3 and 4). Fig. 3 shows geometrically inequivalent Cu ions (Sbp–Cu1 in green; Sp–Cu2 in blue) and their corresponding dihedral angles (α, in orange) defined within **1**. The α parameter from the planes defined by the square-based pyramidal Cu1 atom (green) and O105–Gd1–O109 (pink) display values above 40° (see Table S3†). In contrast, α values related to planes described by the square-based Cu2 atom (blue) and O204–Gd1–O209 (pink) are much smaller (ranging from 18.5 to 19.9°, see Table S3 in ESI†). Consequently, we anticipate a stronger ferromagnetic Sp–Cu···Gd exchange interaction ($\mathcal{J}_2$ in the magnetic model from Fig. 4) compared to that displayed for Sbp–Cu···Gd ($\mathcal{J}_1$). These conclusions are in good agreement with the smaller values of torsion angles for Cu1–O···O–Ln ($\theta \sim 135°$; see Table S3†) compared to those displayed for Cu2–O···O–Ln ($\theta \sim 160°$).[3c,20] Further interpretation of the different intramolecular Cu···Cu and Cu···Gd exchange interactions will be developed in the computational section.

The dynamic magnetic properties of **2** and **3** were measured to check for any slow relaxation of the magnetisation (see ESI†). Complex **2** (Tb) displays the onset of an out-of-phase χ'' ac signal in zero dc field, however, the signal is very weak, and no enhancement was observed despite the application of an external dc field (see Fig. S3†).[21] Complex **3** (Dy) shows a stronger χ'' signal in zero dc field, which is improved in an external dc field (see Fig. S3†), but it was not possible to shift the χ'' signal enough to see any maxima and we calculate a small spin reversal barrier of ~10 K (see Fig. S4 and Table S5†).[22] Further details are provided in the ESI.†

Electronic structure calculations

Electronic structure calculations have been carried out to analyse the different exchange pathways between the metal centres within **1** {$GdCu_4$} and **4** {$LaCu_4$}. The Hamiltonian used to calculate the exchange interactions is $\mathcal{H} = -\sum_{a<b}\left(J_{ab}\hat{S}_a\hat{S}_b\right)$. (see further computational details in the Experimental section). As indicated in Fig. 4, compound **1** presents four different exchange pathways: $\mathcal{J}_1$ between Gd1–Cu1 and Gd1–Cu3, $\mathcal{J}_2$ between Gd1–Cu2 and Gd1–Cu4, $\mathcal{J}_3$ between Cu(II) in the *cis* configuration and $\mathcal{J}_4$ between those in the *trans* configuration. In compound **4**, because La^{3+} has no f electrons, no exchange pathway is observed between La···Cu, and only $\mathcal{J}_3$ and $\mathcal{J}_4$ are considered (Fig. S5,† right).

For **1**, the computed values for the Gd···Cu coupling constants ($\mathcal{J}_1 = -0.53$ cm^{-1} and $\mathcal{J}_2 = +2.55$ cm^{-1}; see Table 2) are in good agreement with exchange interactions previously reported for other Gd/Cu complexes.[3a,c,23] As mentioned earlier, the dihedral angle (α) is defined by the planes formed by the atoms involved in the magnetic exchange (Fig. 3). The computed $\mathcal{J}_1$, $\mathcal{J}_2$ values are also consistent with the structural features related to the Cu–Gd dihedral angles discussed previously, *i.e.* the smaller dihedral angle, the stronger the tendency to be ferromagnetically coupled (*vide supra*). Therefore, the magnetic exchange interaction between Cu(Sp)···Gd (Cu2, Cu4 in Fig. 4) is ferromagnetic ($\mathcal{J}_2 = +2.55$ cm^{-1}), in good agreement with the relatively small α angle (19.4°) and large torsion angle (160.6°). In contrast, the exchange interaction between Cu(Sbp)···Gd (Cu1, Cu3 in Fig. 4) is weakly antiferromagnetic ($\mathcal{J}_2 = -0.53$ cm^{-1}), which is consistent with the large α value (44.2°) and the relatively smaller torsion angle (135.8°). The increase in the ferromagnetic character of the Gd–Cu interaction can be also traced back to the increasing co-planarity between the Cu, O and Gd atoms, as has been reported both computationally[3c] and experimentally (see Table S6 and Fig. S6†). The exchange interactions between Cu(II) ions ($\mathcal{J}_3$, $\mathcal{J}_4$) differ between **1** and **4**. The spin density plots for **1** and **4** show the different charge distribution within the molecule as a consequence of the replacement of the central Ln ion (Fig. 5). In **1** the spin density is delocalised over the molecule, whereas the spin density for **4** is confined to the Cu(II) coordination environment, due to the lack of f electrons in the La(III) ion. This is consistent with the stronger calculated values for $\mathcal{J}_3$ and $\mathcal{J}_4$ corresponding to the different intramolecular Cu···Cu interactions for **1** ($\mathcal{J}_3 = +1.74$ cm^{-1}, $\mathcal{J}_4 = -0.44$ cm^{-1}) compared to those for **4** ($\mathcal{J}_3 = -0.15$ cm^{-1}, $\mathcal{J}_4 = -0.09$ cm^{-1}).

In addition to these intramolecular interactions, the sharp drop in the $\chi_M T$ value at low temperatures for **1** and **4** suggests the presence of some intermolecular interactions. The shortest intermolecular Cu···Cu′ interaction (where Cu, Cu′ belong to

Table 2 Summary of calculated Ln···Cu and Cu···Cu exchange interactions for **1** {$GdCu_4$} and **4** {$LaCu_4$} from DFT studies

Coupling constants	**1** (Gd)	Cu–O···O–Ln	Dihedral angle α	**4** (La)
$\mathcal{J}_1$ (Ln···Cu)	−0.53 cm^{-1}	135.8°	44.2°	—
$\mathcal{J}_2$ (Ln···Cu)	+2.55 cm^{-1}	160.6°	19.4°	—
$\mathcal{J}_3$ (Cu···Cu)	+1.74 cm^{-1}	—	—	−0.15 cm^{-1}
$\mathcal{J}_4$ (Cu···Cu)	−0.44 cm^{-1}	—	—	−0.09 cm^{-1}

Open Access Article. Published on 02 February 2023. Downloaded on 10/19/2023 4:08:06 PM.
This article is licensed under a Creative Commons Attribution 3.0 Unported Licence.

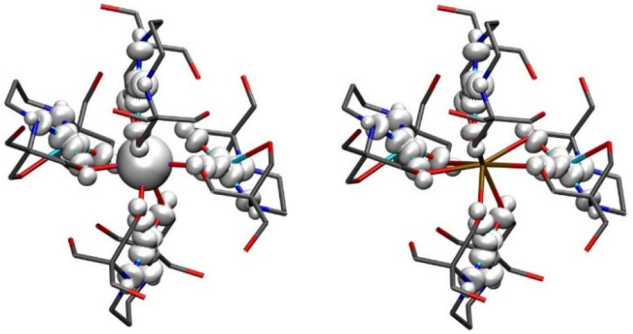

Fig. 5 DFT computed spin density plots for {$GdCu_4$} (**1**, left) and {$LaCu_4$} (**4**, right).

different molecules), in both **1** (7.561(1) Å) and **4** (7.436(1) Å) is between the Cu(Sbp) centres (see Fig. S7†). The Cu···Cu′ interaction between the Cu(Sp) centres (see Fig. S8†) is 7.821(1) Å in **1** and 7.710(1) Å in **4**. A fit of the magnetic susceptibility data of **1** and **4** was then performed to investigate the intermolecular interactions present in the crystal structures. Therefore, the value of the intermolecular interaction ($z\mathcal{J}'$) for **1** and **4** was extracted by using the program PHI,[24] giving consideration to the magnetic models and by applying the spin Hamiltonians displayed in Fig. S5.† The DFT computed $\mathcal{J}$ values (see Table 2) were included as fixed parameters during the fit. The g_{Cu}, g_{Gd} parameters were fixed at 2.11 and 2, respectively, during the fit and a temperature-independent paramagnetic term of TIP = 2×10^{-4} cm^3 mol^{-1} was also included. The best results (*vide supra*) give $z\mathcal{J}' = -0.027 \pm 0.001$ cm^{-1} and -0.030 ± 0.008 cm^{-1} for **1** and **4**, respectively (see solid lines in Fig. 2). These results are consistent with the similar Cu···Cu′ intermolecular interactions in **1** and **4**.

Conclusions

We have synthesised a family of new 3d–4f systems $[LnCu_4(H_4L)_4](Cl)_2(ClO_4)\cdot 6CH_3OH$ (Ln = Gd (**1**), Tb (**2**), Dy (**3**) or La (**4**)). The use of typically non-coordinating and/or monodentate co-ligands (ClO_4^- and Cl^-) promotes the assembly of four {$Cu(H_4L)$} units around the central lanthanide ion, giving a four-blade propeller topology. The analysis of the dihedral angles (α) related to the Cu–Gd ions in **1** suggests different magnetic exchange pathways depending on the Cu(II) environment. The square planar Cu(II) ions are more likely to be ferromagnetically coupled to Gd(III) (small α), whereas the square-based pyramidal Cu(II) ions would tend to be coupled antiferromagnetically (albeit weakly) with Gd(III) (large α). Electronic structure calculations (DFT) on **1** support these findings giving two different Gd···Cu coupling constants ($\mathcal{J}_1 = -0.53$ cm^{-1} and $\mathcal{J}_2 = +2.55$ cm^{-1}) as well as two Cu···Cu coupling constants for the Cu centres located either *cis*- or *trans*- to each other. The calculated spin density shows a different charge delocalisation between **1** (Gd) and **4** (La) due to the replacement of the paramagnetic Gd(III) ion by the diamagnetic La(III) ion, which may explain the weaker calculated *cis*-Cu and *trans*-Cu coupling constants in **4**.

Author contributions

MHO carried out the synthesis and sample characterisation; crystallographic measurements, advised by CW, and magnetic measurements, advised by HO and MM. DFT calculations were carried out by JC and ER. MM devised and supervised the project. The manuscript was written by MHO and MM with input from all authors.

Conflicts of interest

There are no conflicts to declare.

Acknowledgements

We thank the University of Glasgow for financial support and Mr James Gallagher for his assistance in performing the EDX experiments. MHO is thankful to the Japan Society for the Promotion of Science (JSPS) for the Short-Term Pre/Postdoctoral Fellowship for International Research. JC and ER thank the Spanish Ministerio de Ciencia e Innovación for the Maria de Maeztu Excellence Accreditation (CEX2021-001202-M). ER thanks the Spanish Ministerio de Ciencia e Innovación (PID2021-122464NB-I00), and Generalitat de Catalunya for an ICREA Academia award and for the SGR2017-1289 grant. JC thanks the Spanish MICINN for a Ramón y Cajal research contract (RYC2018- 024692-I) and the Spanish MICINN research grant (PID2020-115165GB-I00).

References

1 (*a*) H. Kaemmerer, A. Baniodeh, Y. Peng, E. Moreno-Pineda, M. Schulze, C. E. Anson, W. Wernsdorfer, J. Schnack and A. K. Powell, *J. Am. Chem. Soc.*, 2020, **142**, 14838–14842; (*b*) R. Alotaibi, J. M. Fowler, S. J. Lockyer, G. A. Timco, D. Collison, J. Schnack and R. E. P. Winpenny, *Angew. Chem., Int. Ed.*, 2021, **60**, 9489–9492; (*c*) M. Coletta, R. McLellan, S. Sanz, K. J. Gagnon, S. J. Teat, E. K. Brechin and S. J. Dalgarno, *Chem. – Eur. J.*, 2017, **23**, 14073–14079; (*d*) V. A. Milway, F. Tuna, A. R. Farrell, L. E. Sharp, S. Parsons and M. Murrie, *Angew. Chem., Int. Ed.*, 2013, **52**, 1949–1952.

2 (*a*) S. Osa, T. Kido, N. Matsumoto, N. Re, A. Pochaba and J. Mrozinski, *J. Am. Chem. Soc.*, 2004, **126**, 420–421; (*b*) T. Hamamatsu, K. Yabe, M. Towatari, S. Osa, N. Matsumoto, N. Re, A. Pochaba, J. Mrozinski, J.-L. Gallani, A. Barla, P. Imperia, C. Paulsen and J.-P. Kappler, *Inorg. Chem.*, 2007, **46**, 4458–4468; (*c*) L. Rosado Piquer and E. C. Sanudo, *Dalton Trans.*, 2015, **44**, 8771–8780; (*d*) A. B. Canaj, D. I. Tzimopoulos,

 This journal is © The Royal Society of Chemistry 2023

Open Access Article. Published on 02 February 2023. Downloaded on 10/19/2023 4:08:06 PM. This article is licensed under a Creative Commons Attribution 3.0 Unported Licence.

M. Siczek, T. Lis, R. Inglis and C. J. Milios, *Inorg. Chem.*, 2015, **54**, 7089–7095; (*e*) A. Dey, P. Bag, P. Kalita and V. Chandrasekhar, *Coord. Chem. Rev.*, 2021, **432**, 213707.

3 (*a*) J.-P. Costes, F. Dahan and A. Dupuis, *Inorg. Chem.*, 2000, **39**, 5994–6000; (*b*) T. Shimada, A. Okazawa, N. Kojima, S. Yoshii, H. Nojiri and T. Ishida, *Inorg. Chem.*, 2011, **50**, 10555–10557; (*c*) J. Cirera and E. Ruiz, *C. R. Chim.*, 2008, **11**, 1227–1234; (*d*) C. Benelli and D. Gatteschi, *Chem. Rev.*, 2002, **102**, 2369–2388; (*e*) R. E. P. Winpenny, *Chem. Soc. Rev.*, 1998, **27**, 447–452; (*f*) N. Ahmed, T. Sharma, L. Spillecke, C. Koo, K. Uddin Ansari, S. Tripathi, A. Caneschi, R. Klingeler, G. Rajaraman and M. Shanmugam, *Inorg. Chem.*, 2022, **61**, 5572–5587.

4 A. Bencini, C. Benelli, A. Caneschi, R. L. Carlin, A. Dei and D. Gatteschi, *J. Am. Chem. Soc.*, 1985, **107**, 8128–8136.

5 (*a*) M. Murrie, *Polyhedron*, 2018, **150**, 1–9; (*b*) G. A. Craig, G. Velmurugan, C. Wilson, R. Valiente, G. Rajaraman and M. Murrie, *Inorg. Chem.*, 2019, **58**, 13815–13825.

6 M. Heras Ojea, V. A. Milway, G. Velmurugan, L. H. Thomas, S. J. Coles, C. Wilson, W. Wernsdorfer, G. Rajaraman and M. Murrie, *Chem. – Eur. J.*, 2016, **22**, 12839–12848.

7 L. Palatinus and G. Chapuis, *J. Appl. Crystallogr.*, 2007, **40**, 786–790.

8 G. Sheldrick, *Acta Crystallogr., Sect. C: Struct. Chem.*, 2015, **71**, 3–8.

9 O. V. Dolomanov, L. J. Bourhis, R. J. Gildea, J. A. K. Howard and H. Puschmann, *J. Appl. Crystallogr.*, 2009, **42**, 339–341.

10 M. Heras Ojea, G. Lorusso, G. A. Craig, C. Wilson, M. Evangelisti and M. Murrie, *Chem. Commun.*, 2017, **53**, 4799–4802.

11 (*a*) E. Ruiz, P. Alemany, S. Alvarez and J. Cano, *J. Am. Chem. Soc.*, 1997, **119**, 1297–1303; (*b*) E. Ruiz, J. Cano, S. Alvarez and P. Alemany, *J. Comput. Chem.*, 1999, **20**, 1391–1400; (*c*) E. Ruiz, A. Rodriguez-Fortea, J. Cano, S. Alvarez and P. Alemany, *J. Comput. Chem.*, 2003, **24**, 982–989.

12 M. J. Frisch, G. W. Trucks, H. B. Schlegel, G. E. Scuseria, M. A. Robb, J. R. Cheeseman, G. Scalmani, V. Barone, B. Mennucci, G. A. Petersson, H. Nakatsuji, M. Caricato, X. Li, H. P. Hratchian, A. F. Izmaylov, J. Bloino, G. Zheng, J. L. Sonnenberg, M. Hada, M. Ehara, K. Toyota, R. Fukuda, J. Hasegawa, M. Ishida, T. Nakajima, Y. Honda, O. Kitao, H. Nakai, T. Vreven, J. A. Montgomery Jr., J. E. Peralta, F. Ogliaro, M. J. Bearpark, J. Heyd, E. N. Brothers, K. N. Kudin, V. N. Staroverov, R. Kobayashi, J. Normand, K. Raghavachari, A. P. Rendell, J. C. Burant, S. S. Iyengar, J. Tomasi, M. Cossi, N. Rega, N. J. Millam, M. Klene, J. E. Knox, J. B. Cross, V. Bakken, C. Adamo, J. Jaramillo, R. Gomperts, R. E. Stratmann, O. Yazyev, A. J. Austin, R. Cammi, C. Pomelli, J. W. Ochterski, R. L. Martin, K. Morokuma, V. G. Zakrzewski, G. A. Voth, P. Salvador, J. J. Dannenberg, S. Dapprich, A. D. Daniels, Ö. Farkas, J. B. Foresman, J. V. Ortiz, J. Cioslowski and D. J. Fox, in *Gaussian 09, Vol*, Gaussian, Inc., Wallingford, CT, USA, 2009.

13 A. D. Becke, *J. Chem. Phys.*, 1993, **98**, 5648–5652.

14 A. Schafer, C. Huber and R. Ahlrichs, *J. Chem. Phys.*, 1994, **100**, 5829–5835.

15 (*a*) M. Douglas and N. M. Kroll, *Ann. Phys.*, 1974, **82**, 89–155; (*b*) B. A. Hess, *Phys. Rev. A*, 1985, **32**, 756–763.

16 (*a*) M. Pinsky and D. Avnir, *Inorg. Chem.*, 1998, **37**, 5575–5582; (*b*) D. Casanova, M. Llunell, P. Alemany and S. Alvarez, *Chem. – Eur. J.*, 2005, **11**, 1479–1494.

17 A. W. Addison, T. N. Rao, J. Reedijk, J. van Rijn and G. C. Verschoor, *J. Chem. Soc., Dalton Trans.*, 1984, 1349–1356.

18 P. Richardson, D. I. Alexandropoulos, L. Cunha-Silva, G. Lorusso, M. Evangelisti, J. Tang and T. C. Stamatatos, *Inorg. Chem. Front.*, 2015, **2**, 945–948.

19 (*a*) P. de Hoog, P. Gamez, O. Roubeau, M. Lutz, W. L. Driessen, A. L. Spek and J. Reedijk, *New J. Chem.*, 2003, **27**, 18–21; (*b*) M. Heras Ojea, C. Wilson, S. J. Coles, F. Tuna and M. Murrie, *Dalton Trans.*, 2015, **44**, 19275–19281.

20 (*a*) F. Yan and Z. Chen, *J. Phys. Chem. A*, 2000, **104**, 6295–6300; (*b*) J. Paulovič, F. Cimpoesu, M. Ferbinteanu and K. Hirao, *J. Am. Chem. Soc.*, 2004, **126**, 3321–3331.

21 S. L. Castro, Z. Sun, C. M. Grant, J. C. Bollinger, D. N. Hendricksonand and G. Christou, *J. Am. Chem. Soc.*, 1998, **120**, 2365–2375.

22 J. Bartolomé, G. Filoti, V. Kuncser, G. Schinteie, V. Mereacre, C. E. Anson, A. K. Powell, D. Prodius and C. Turta, *Phys. Rev. B: Condens. Matter Mater. Phys.*, 2009, **80**, 014430.

23 (*a*) G. Rajaraman, F. Totti, A. Bencini, A. Caneschi, R. Sessoli and D. Gatteschi, *Dalton Trans.*, 2009, 3153–3161; (*b*) J.-P. Costes, F. Dahan, A. Dupuis and J.-P. Laurent, *Inorg. Chem.*, 2000, **39**, 169–173.

24 N. F. Chilton, R. P. Anderson, L. D. Turner, A. Soncini and K. S. Murray, *J. Comput. Chem.*, 2013, **34**, 1164–1175.